PHOTONICS Research

Multiple resonant excitations of surface plasmons in a graphene stratified slab by Otto configuration and their independent tuning

Jin Yao,[1] Ying Chen,[1] Longfang Ye,[1] Na Liu,[1] Guoxiong Cai,[1,*] and Qing Huo Liu[2]

[1]Institute of Electromagnetics and Acoustics, and Department of Electronic Science, Xiamen University, Xiamen 361005, China
[2]Department of Electrical and Computer Engineering, Duke University, Durham, North Carolina 27708, USA
*Corresponding author: gxcai8303@xmu.edu.cn

Received 19 May 2017; revised 20 June 2017; accepted 27 June 2017; posted 27 June 2017 (Doc. ID 295192); published 26 July 2017

Multiple resonant excitations of surface plasmons in a graphene stratified slab are realized by Otto configuration at terahertz frequencies. The proposed graphene stratified slab consists of alternating dielectric layers and graphene sheets, and is sandwiched between a prism and another semi-infinite medium. Optical response and field distribution are determined by the transfer matrix method with the surface current density boundary condition. Multiple resonant excitations appear on the angular reflection spectrum, and are analyzed theoretically via the phase-matching condition. Furthermore, the effects of the system parameters are investigated. Among them, the Fermi levels can tune the corresponding resonances independently. The proposed concept can be engineered for promising applications, including angular selective or multiplex filters, multiple channel sensors, and directional delivery of energy.

OCIS codes: (240.6680) Surface plasmons; (230.4170) Multilayers; (230.5480) Prisms; (350.2450) Filters, absorption; (060.4230) Multiplexing.

https://doi.org/10.1364/PRJ.5.000377

1. INTRODUCTION

As a 2D material composed of carbon atoms arranged in a honeycomb lattice, graphene possesses extraordinary electric and photonic properties, which attract enormous research interest [1]. Among them, the graphene surface plasmon (GSP) has been predicted and experimentally observed to exhibit strong field confinement and relatively low propagation loss, as well as fast and efficient electrical tunability over a broad wavelength band [2,3]. Terahertz to mid-IR applications of GSPs have been intensively investigated, e.g., optical modulation [4], on-chip interconnects [5], and bio-sensing [6].

However, it is challenging to directly couple externally incident IR radiation to a GSP mode, due to the large mismatch between their wave vectors. Techniques to overcome this mismatch include near-field excitation using a sharp tip of a scanning near-field optical microscope [7], the diffraction orders provided by diffractive gratings or period lattice geometry [8,9], and the tunneling of evanescent waves originating from the attenuated total reflectance (ATR) of light in a prism with a high refractive index [10]. Without the sophisticated fabrication of nanostructures, the prism-based ATR technique receives wide interest in science and engineering. Resonant excitations will be observed from the reflection dip on the angular or frequency spectrum whenever the wave vectors match each other. Due to the 2D nature of graphene, Otto configuration is preferred over Kretschmann ones. Transverse magnetic (TM) GSP excitation has been theoretically investigated on the thickness of a low-index dielectric gap in an Otto configuration [11], the Fermi level, and the number of layers of graphene [12]. Novel photonic devices, e.g., optoelectronic switches [13], polarizers [14], filters [15], and optical logical bistable devices [16], have been proposed and realized.

On the other hand, multiple channels and multiplexing operation are highly required in systems including optical communication, spectroscopy and sensors, absorbers, and filters. Traditional techniques were limited by their tunability [17]. In recent years, multiple channels featuring graphene's tunability and its plasmonic resonance have been drawing considerable attention. Plasmonic crystals consisting of graphene periodic anti-dot arrays have been measured to have multiple resonances on the transmission spectrum, which correspond to the excitation of different branches of the GSP dispersion curves inherent to the periodic structures [18]. Meanwhile, by engineering the widths of multiple graphene nanoribbons, which are vertically or horizontally allocated in a metamaterial unit cell, multiple spectral responses have emerged. They led to applications of multiple electromagnetically induced transparency-like effects [19] and multiport switches and filters [20]. Furthermore,

double Fano resonances have been realized by the interference between the plasmonic resonances arising from a graphene disk and a gold ring [21].

However, multiple resonances in these devices tended to act simultaneously, since they were of different orders of the GSP modes. The tuning of one resonance would accordingly influence the others. To address this problem, metamaterial resonators of different sizes were placed onto the interdigitated graphene fingers to enable independently tunable dual-band resonances [22], while a free-standing graphene hybrid slab could support the independent tuning of double plasmonic waves on graphene above and below their shared grating [23].

In this paper, we present the concept of multiple GSP resonant excitations via Otto configuration and their independent tuning in a graphene stratified slab at terahertz frequencies. The proposed stratified slab is formed by arranging alternating dielectric layers and graphene sheets. A high refractive index prism is then placed on top of the graphene stratified slab to couple the external incident light into the multiple GSP resonances. An Otto configuration is constructed. By varying incident angles, phase-matching conditions can be satisfied, and multiple resonant excitations can be realized on the angular reflection spectrum. We first investigate the case of double GSP resonant excitations, and discuss the effects of the system parameters, e.g., the Fermi levels of the graphene layers and the refractive index and geometrical parameters of the dielectric layers. Among them, the Fermi level can tune the double resonances independently. Then, the concept is generalized to a multiple scenario. The results indicate that the proposed concept can be engineered for promising applications, including angular selective or multiplex filters and modulators, multiple channel sensors, and directional delivery of energy.

2. DOUBLE RESONANT EXCITATIONS AND INDEPENDENT TUNING

A. Model Configuration and Operation Principle

The independent excitation and tuning of double GSPs is investigated in this section. As shown in Fig. 1, the proposed graphene stratified slab is formed by two sets of alternating dielectric layers and graphene sheets. The refractive index and the thickness of the dielectric layer are n_1 (n_2) and d_1 (d_2), respectively. All dielectric layers are assumed to be nonpolar to ignore the effects of surface optical phonons [12,24]. The stratified slab is then sandwiched between the prism and another semi-infinite dielectric medium (bottom part of the figure) with $n_a = 1$. The refractive index of the prism ($n_p = 4$ as a Germanium prism) is set to be higher than those of all dielectrics in the system. One reason for the high index is to generate tunneling evanescent waves by ATR, and another is to provide a sufficient wave vector so that the phase-matching condition can be satisfied. It is worth pointing out that the first dielectric layer n_1 from the proposed stratified slab is shared by graphene A as upper cladding and the Otto configuration as a coupling gap. A TM-polarized plane wave is incident on the prism (along the $+z$ direction) at an angle of θ.

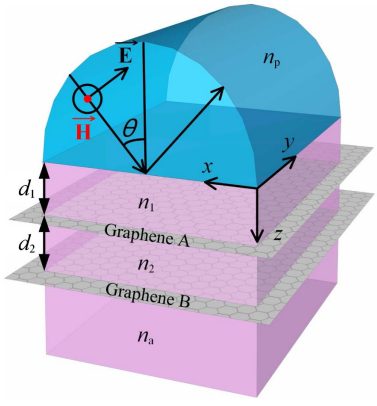

Fig. 1. Schematic of the proposed graphene stratified slab cladded by the prism and another semi-infinite dielectric medium. Double GSP resonances can be excited by Otto configuration under TM-wave incidence.

A transfer matrix method with the surface current density boundary condition (TMM-SCBC) is adopted to analyze the proposed system [25]. Instead of employing equivalent permittivity to describe the electromagnetic behavior of graphene [26,27], this method uses its surface conductivity. A surface current density can thus be introduced into the Maxwell equation by Ohm's law without the artificial assumption of graphene's thickness. The TMM-SCBC method provides an accurate and efficient technique for simulating a graphene-based stratified slab. Key equations for the TMM-SCBC method are listed, and the validation of the optical response and the electromagnetic distribution are presented in Appendix A.

At terahertz frequencies, the interband transitions have a negligible contribution due to Pauli blocking, and the surface conductivity of graphene is dominated by intraband transitions, following a Drude-like expression:

$$\sigma(\omega) = \frac{e^2 E_F}{\pi\hbar}\frac{i}{\omega + i\tau^{-1}}, \tag{1}$$

where e is the electric charge, $\hbar$ is the reduced Planck constant, E_F is the Fermi level of graphene, and τ is the phenomenological carrier relaxation time. To begin with, $E_F = 0.3$ eV and $\tau = 6$ ps for both graphene layers in Fig. 1. The corresponding carrier mobility μ can then be deduced to be 200000 $\mathrm{cm^2 \cdot (V^{-1} \cdot s^{-1})}$ by the relation $\mu = \tau(ev_f^2)/E_F$, where v_f is the Fermi velocity. It is one order smaller than the theoretically estimated value [28], and falls within the range of currently experimental capacity [29].

In order to better demonstrate the concept of double resonant excitations of GSP modes, the dielectric layers are assigned to be $n_1 = 1.8$ and $n_2 = 1.4$, while their thicknesses are $d_1 = 28$ μm and $d_2 = 63$ μm, respectively. Discussion about refractive index and geometrical dependence of the double resonances can be found in Subsection 2.C. The optical responses with respect to the incident angle θ are then plotted in Fig. 2(a) at frequency $f = 1$ THz. Three dips appear on the angular reflection spectrum. Due to the zero transmittance for incident angles larger than the critical angle, the absorption spectrum has three peaks on it. Among them, the reflection dips labeled I (51.2°) and II (29.0°) are the resonant excitations corresponding to the GSP modes supported by graphene A and B, respectively, while dip III is, in fact, the coherent absorption of graphene [11,30]. The coherent absorption results from the

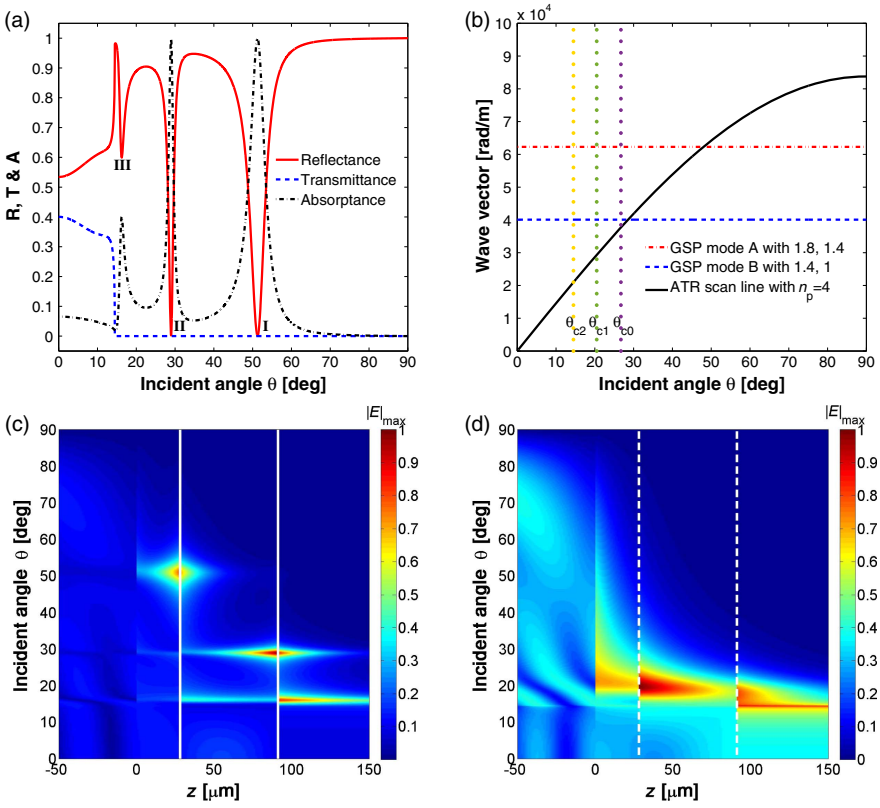

Fig. 2. (a) Optical responses of the proposed graphene stratified slab with respect to the incident angle θ at frequency $f = 1$ THz, (b) schematic diagram depicting the phase-matching mechanism for double resonant excitations of GSP modes. The three dotted lines indicate three critical angles for ATRs occurring at interfaces of $n_p - n_1$, $n_1 - n_2$, and $n_2 - n_a$, respectively. (c) Electric field distributions along the z direction for light with varying incident angle θ. The white solid lines denote two graphene sheets placed at the interfaces of the dielectric layers. The prism occupies the region $z < 0$. (d) Electric field distributions in the absence of graphene sheets. The white dashed lines indicate the interfaces of dielectric layers, except for the $n_p - n_1$ one, which is located at $z = 0$.

optical interference in the dielectric layers, which produces a large electric field at their outer interfaces. While the graphene sheets are exactly located at the interfaces, dissipation arises from their surface conductivity by Ohm's law.

The origin of resonant excitations I and II can be confirmed by the phase-matching theory, as depicted in Fig. 2(b). For the plasmonic TM mode in a GSP waveguide, the propagation constant k_{sp} can be determined by [31]:

$$\frac{\varepsilon_{r1}}{\sqrt{k_{sp}^2 - \frac{\varepsilon_{r1}\omega^2}{c^2}}} + \frac{\varepsilon_{r2}}{\sqrt{k_{sp}^2 - \frac{\varepsilon_{r2}\omega^2}{c^2}}} = \frac{-i\sigma(\omega)}{\omega\varepsilon_0}, \tag{2}$$

where ω is the angular frequency of light, ε_0 is the vacuum permittivity, ε_{r1} and ε_{r2} are the relative permittivities of the cladding materials, and $\sigma(\omega)$ is the surface conductivity of graphene, which is described by Eq. (1). At terahertz frequencies, this is a transcend equation, and it can be solved numerically. The real parts of k_{sp} for GSP modes A and B were thus plotted in Fig. 2(b). It should be noted that they are straight lines, since Eq. (2) is the eigen dispersion equation, which is irrelevant to the incident angles of external light. An ATR scan line of the prism was then plotted [Fig. 2(b)], which is the in-plane component of the wave vector for incident light in a prism,

$$k_x = n_p k_0 \sin(\theta), \tag{3}$$

where k_0 is the wave vector in vacuum. Right after the critical angle θ_{c0}, the ATR scan line crosses the k_{sp} lines at 48.0° and 28.5°, respectively. The theoretically predicted results find consistency with the angles read from optical responses in Fig. 2(a). This indicates that dips I and II are the resonant excitations of GSP modes supported by graphene A and B, respectively. When phase-matching conditions are satisfied, the energy of external propagating light tunnels to the GSP waveguide modes via evanescent waves originating from the ATR, leading to the emergence of reflectance minima.

On the other hand, it can be seen in Fig. 2(a) that the width of resonance I is broader than that of resonance II. This is related to the imaginary part of k_{sp}, which characterizes the radiative damping of a GSP mode. From Eq. (2), GSP mode A has a larger imaginary part of k_{sp}, leading to the broadening of its corresponding resonant excitation [12].

Furthermore, Fig. 2(c) shows the field patterns of the proposed stratified slab, with the electric field distributions along the z direction while light varies its incident angle θ. The field pattern for dip III has a different distribution compared to those of dip I and II, which is first-order interference in dielectric layer 2 [30]. Next we ignore dip III. Typical field patterns of the GSP mode emerge at angles of 51.2° and 29.0°, corresponding to reflection dips I and II, respectively. This suggests a

novel application where the light energy can be delivered to different graphene layers when the incident angle is selectively changed. Meanwhile, for a specific resonant angle in Fig. 2(c), the field concentrates around its corresponding graphene layer and decays exponentially away from it, which is analogous to the standard eigenmode pattern of a GSP waveguide [10,31]. There is no disturbance or coupling to colleague graphene due to the graphene transparency and the tight field confinement of the GSP modes [23]. Together with the phase matching in Fig. 2(b), the possibility of independent manipulation of individual resonant excitations can be realized, which will be investigated in Subsection 2.B.

For the sake of comparison, electric field distributions in the absence of graphene sheets are presented in Fig. 2(d) as well. Instead of confined GSP modes, evanescent waves emerge at three interfaces of dielectric layers when θ is larger than their corresponding critical angles. The introduction of graphene gives rise to the resonant excitations on the angular reflection spectrum in Fig. 2(a), as well as the standard GSP mode pattern in the proximity of graphene, as shown in Fig. 2(c). On the other hand, we now revisit the critical angles in our system. Though there is only one critical angle read on the angular transmission/reflection spectrum, three total internal reflections (θ_{c0}, θ_{c1}, and θ_{c2}) happen on their corresponding interfaces ($n_p - n_1$, $n_1 - n_2$, and $n_2 - n_a$), as shown in Figs. 2(b) and 2(d). Each evanescent wave can excite GSP modes as long as the graphene layers are located within the tunneling range and the phase-matching conditions are fulfilled. However, we choose the one generated on the $n_p - n_1$ interface, where no graphene layer is located, to act as the agency between the external propagating light and the GSP modes. This configuration will facilitate independent tuning by the Fermi level of the graphene. In the following subsection, we investigate the double resonant excitations, including their resonant angles and line shapes, as a function of Fermi levels.

B. Independent Tuning by Fermi Level

Independent tuning was investigated by adjusting the Fermi level of each graphene layer separately. Figure 3(a) shows the angular reflection spectra of the proposed graphene stratified slab with various Fermi levels for each graphene layer. Parameters are kept the same as those in Fig. 2 unless otherwise stated. First, the Fermi level doped on graphene A is fixed at $E_{\mathrm{FA}} = 0.3$ eV, while that of graphene B drops from 0.5 to 0.3 eV in steps of 0.1 eV. It can be seen that the resonant angle θ_{RII} of dip II is increased with the reduction of E_{FB}, while dip I remains the same, as indicated by the black dotted line. Similarly, θ_{RI} of dip I decreases with a rising of E_{FA}, while θ_{RII} remains constant, as E_{FB} is unchanged during this process, as indicated by the black dashed line. Separate tunability of the double resonant excitations is realized by modulating the Fermi level of the corresponding graphene layer. Figure 3(b) provides the case where the operation frequency f is 3 THz and a higher graphene loss of $\tau = 1$ ps is used. The thicknesses of the dielectric layers are optimized to be $d_1 = 8$ μm and $d_2 = 19$ μm, leaving their refractive indices the same as those in Fig. 2.

We go back to $f = 1$ THz and analyze its broad tuning range by Fermi levels. Figure 4(a) shows the resonant angles as a function of their corresponding Fermi levels. Theoretically estimated results determined by the phase-matching mechanism

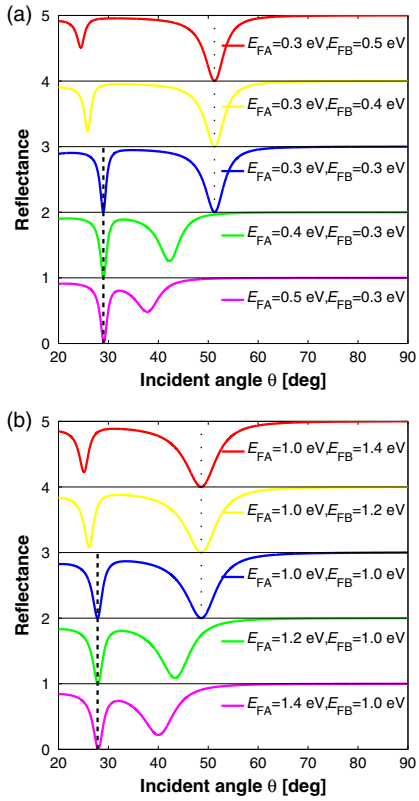

Fig. 3. (a) Angular reflection spectra with various Fermi levels on each graphene layer. The black dotted line indicates the independence of resonant excitation I on Fermi level E_{FB}, while the black dashed line indicates the invariance of resonance II with respect to E_{FA}. (b) Independent excitation and tuning of double resonant excitations with frequency $f = 3$ THz and $\tau = 1$ ps.

in Fig. 2(b) are also presented, which validate those read via optical response. It can be seen in Fig. 4(a) that both resonant angles decrease in an approximately exponential behavior as their corresponding Fermi level increases. Moreover, we also performed the E_{FA} (E_{FB}) tuning under different doping of E_{FB} (E_{FA}), which was not shown here for simplicity. The results indicate that the θ_{RI} (θ_{RII}) dependence on the E_{FA} (E_{FB}) will not be affected by its colleague graphene, suggesting that the two resonances can be tuned independently by their corresponding Fermi level. A broad tuning range is feasible from 90° to the critical angle. Applications such as double-channel angular filters, modulators, and multiplexers can be designed with enhanced flexibility.

However, as the Fermi level is more highly doped, the decrease in the resonant angles slows, and both of them tend to become constant. The reason is that the effective refractive index ($n_{\mathrm{eff}} = k_{\mathrm{sp}}/k_0$) of a GSP waveguide mode gets smaller when the Fermi level increases, as implied by Eq. (2). However, it will not decrease infinitely, because the n_{eff} has to be larger than the refractive indices of the claddings of a GSP waveguide.

Moreover, the line shapes are investigated, which are important parameters for the design of angular filters. The full width at half-maximum (FWHM) and the full height (FH), determined from the Lorentz fit of a resonance on the angular reflection spectrum, are given as a function of Fermi levels

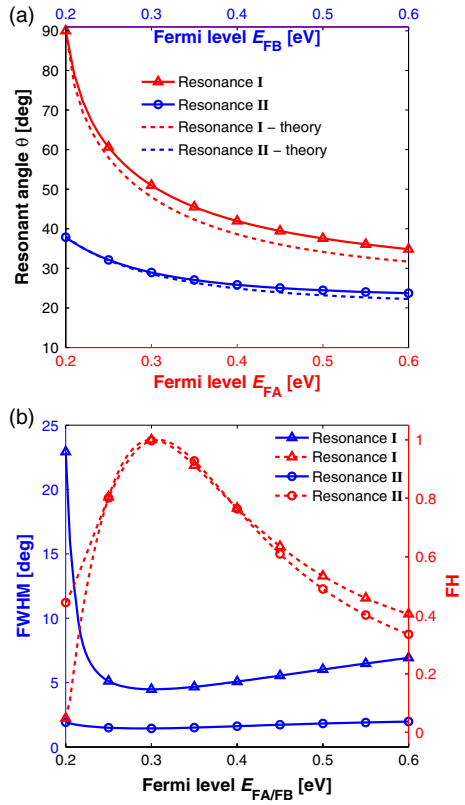

Fig. 4. (a) Dependence of resonant angles on their corresponding Fermi level. Theoretically estimated results are also presented. (b) Dependence of FWHMs and FHs of both resonances on the corresponding Fermi level.

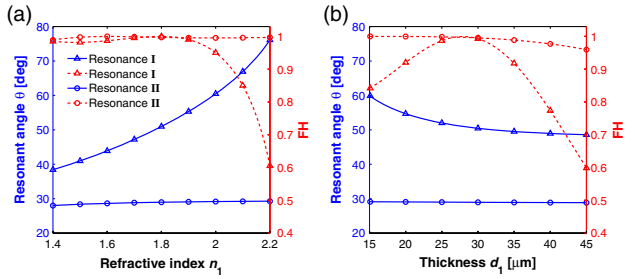

Fig. 5. Dependence of the resonant angle and FH on (a) the refractive index and (b) the thickness of dielectric layer 1. Both resonant excitations are presented.

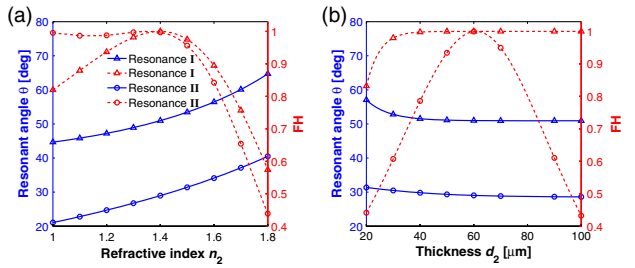

Fig. 6. Dependence of the resonant angle and FH on (a) the refractive index and (b) the thickness of dielectric layer 2. Both resonant excitations are presented.

in Fig. 4(b). Again, the line shape of each resonant excitation is impacted solely by its corresponding Fermi level. On the other hand, it can be seen that both FWHM and FH have optima at a Fermi level of 0.3 eV. However, as the Fermi levels drop, the FWHMs broaden and the FHs are brought down quickly. These indicate the decline of the coupling efficiency between the externally incident light and the GSP mode. Especially for resonant excitation I, the FWHM is 23° and the FH approaches zero when $E_{FA} = 0.2$ eV, and the resulting $\theta_{RI} \approx 90°$. In the next subsection, we will further analyze the influence from the refractive indices and geometrical parameters of the dielectric layers.

C. Effects of Refractive Index and Geometry

Since part of the electromagnetic energy of a GSP mode is located at its cladding dielectrics, the two dielectric layers will tune the two resonant excitations as well. We analyze these effects in Figs. 5 and 6, with both resonances presented. Figure 5(a) shows the dependence of the resonant angle and FH on the refractive index n_1 of dielectric layer 1, while Fig. 5(b) shows the dependence on the thickness d_1. First of all, it can be seen that both an increase in n_1 and a reduction in d_1 cause the resonant angle θ_{RI} of resonance I to increase. The reason lies in the increasing propagating constant k_{sp} with respect to the increasing refractive index of the cladding material, as implied by Eq. (2). To satisfy the phase-matching condition, the incident angle has to increase to provide a larger wave vector. A smaller d_1 means that the high-index prism gets closer to graphene A, and making its cladding equivalent gives it a higher refractive index. Second, the FH of dip I has its optimum within the parameter range of n_1 and d_1. Last, neither θ_{RII} nor FH of resonance II is influenced by n_1 and d_1, since dielectric layer 1 is not the cladding material of graphene B. The slight decline in the FH in Fig. 5(b) for resonance II is due to the increasing distance from graphene B to the ATR interface of $n_p - n_1$. Graphene B goes out of the range of the evanescent wave, and this leads to the downgrading of the coupling efficiency.

Figure 6 shows the dependence of the resonant angle and FH on the refractive index n_2 and the thickness d_2, respectively. The effects of dielectric layer 2 on the resonant angle and FH is similar to those of dielectric layer 1, except that both resonant excitations are involved. This is because dielectric layer 2 serves simultaneously as the cladding of both GSP waveguides A and B. However, as d_2 increases to be thicker than 50 μm, the resonant angle of both resonances I and II, as well as the FH of resonance I, tend to become constant in Fig. 6(b). This is because the coupling between the two GSP modes is avoided, and the effects of graphene B and semi-infinite medium n_a on the bottom cladding n_2 of GSP A gradually disappear. The investigation of the effects of refractive index and geometry provides design references for various applications, though they fail to tune the resonances separately as the parameter of Fermi level does.

3. MULTIPLE RESONANT EXCITATIONS AND INDEPENDENT TUNING

The concept of double resonant excitations can be readily generalized to multiple scenarios. After adding one more set of a dielectric layer and graphene sheet into the proposed stratified slab, triple resonant excitations can be realized. To better demonstrate the phenomenon, the refractive index of the third dielectric layer is optimized to be $n_3 = 1$, with a thickness of $d_3 = 72$ μm, while the Fermi level of graphene C is chosen to be $E_{FC} = 0.3$ eV. Figure 7(a) shows the angular reflection spectrum with three dips on it. The inset also shows the schematic of the graphene stratified slab with three graphene sheets. The resonant angles of the dips satisfy the phase-matching condition, indicating that they are the resonant excitations of the GSP modes in three graphene waveguides, respectively. The details of the calculation are not shown here for simplicity. Figure 7(b) further shows the electric field distributions of the graphene stratified slab for triple plasmonic excitations. Three patterns characterizing the GSP mode distribution appear vividly at their corresponding incident angles. Consequently, an application can be designed to selectively deliver electromagnetic energy into different graphene layers.

To verify the independent tuning for triple resonant excitations, Fig. 8(a) presents the angular reflection spectra with various Fermi levels on each graphene layer. The black dot-dashed, dotted, and dashed lines indicate the starting resonant angles of the three GSP modes with $E_{FA} = E_{FB} = E_{FC} = 0.30$ eV, respectively. In the bottom panel, the Fermi level E_{FA} of graphene A is first tuned from 0.25 to 0.35 eV in steps of 0.05 eV. The resonant angle of dip I is decreased during this process, while dip II and III do not change. The same situation happens for dip II in the middle panel and dip III in the top panel. The three resonances can be separately manipulated by the Fermi level of their corresponding graphene layer. We further extend this concept for quintuple resonant excitations. As demonstrated in Fig. 8(b), quintuple resonances on angular reflection spectra are realized, and dip I is tuned by the Fermi level of graphene A, without disturbance to the other four dips.

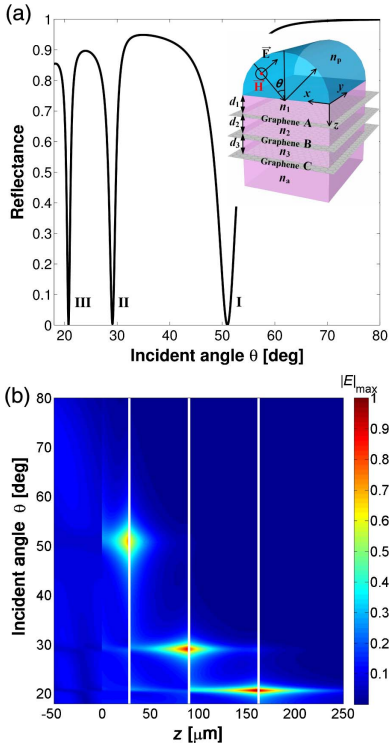

Fig. 7. (a) Angular reflection spectrum with triple resonant excitations. The inset shows the schematic of the graphene stratified slab with three graphene sheets. (b) Electric field distributions of triple resonant excitations. Light is selectively coupled into three different GSP modes by varying the incident angle. The white solid lines denote the three graphene sheets placed at the interfaces of the dielectric layers. The prism occupies the region $z < 0$.

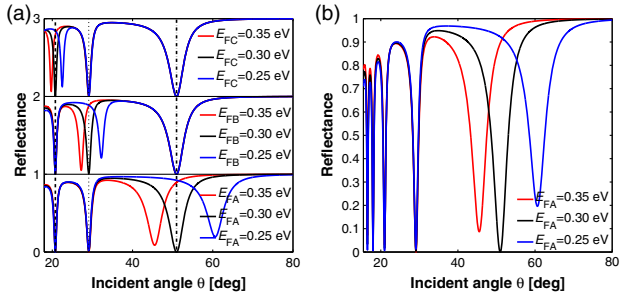

Fig. 8. (a) Angular reflection spectra with various Fermi levels on each graphene layer. The black dot-dashed, dotted, and dashed lines indicate the starting resonant angles of the three GSP modes with $E_{FA} = E_{FB} = E_{FC} = 0.30$ eV, respectively. (b) Angular reflection spectra with quintuple resonant excitations and their independent tuning via the Fermi level of graphene A.

4. CONCLUSION

In summary, we have proposed the independent excitation and tuning of multiple GSPs in a graphene stratified slab via Otto configuration at terahertz frequencies. By varying incident angles, phase-matching conditions can be satisfied, and multiple resonant excitations will emerge as dips on the angular reflection spectrum. The effects of the system parameters are discussed. Among them, the Fermi levels can tune the multiple resonances independently, due to the transparency of graphene and the tight field confinement of GSP modes. The proposed concept can be engineered for promising applications requiring multiple channels or selective energy delivery.

APPENDIX A: KEY EQUATIONS AND VALIDATION

With graphene located at the interface of two dielectric layers, the boundary condition requiring the continuity of the tangential magnetic components (relative to the interface) will be modified to be

$$\mathbf{n} \times (\mathbf{H}_2 - \mathbf{H}_1) = \mathbf{J}_s, \tag{A1}$$

where $\mathbf{n}$ is the unit surface normal and $\mathbf{H}_1$ and $\mathbf{H}_2$ are the magnetic fields at the two sides of the interface. $\mathbf{J}_s$ is the surface current density introduced by applying Ohm's law in the graphene:

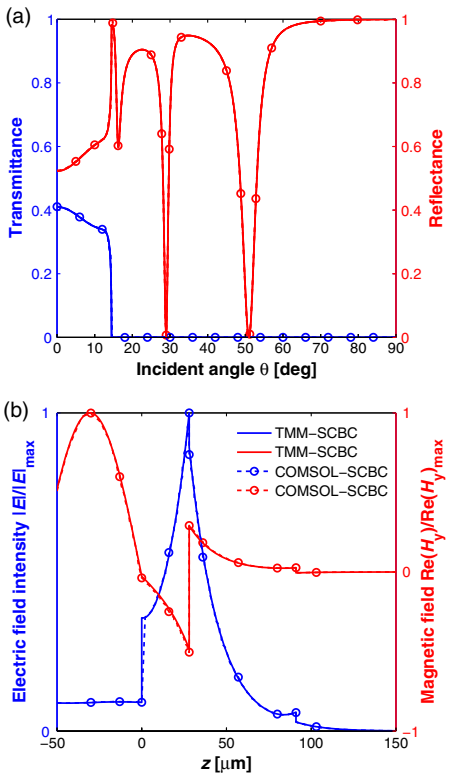

Fig. 9. Validation of (a) angular spectra and (b) electromagnetic distributions comparing results obtained by the TMM-SCBC method and by commercial software COMSOL Multiphysics. An SCBC boundary condition is also employed in the COMSOL simulation. Markers are specific data points to better demonstrate the comparison.

$$\mathbf{J}_s = \sigma \mathbf{E}, \tag{A2}$$

where σ is the surface conductivity of graphene and $\mathbf{E}$ is the electric field at the graphene or the interface.

The standard procedure for the transfer matrix method is adopted, and the transmission matrices as well as the propagation matrix can be determined for both TE and TM incidence. An algorithm is written according to the details in Ref. [25], and electric and magnetic fields are further solved. Figure 9(a) validates the angular reflection and transmission spectra, while Fig. 9(b) validates the field distributions.

Compared to the use of volume permittivity by assuming a finite thickness of graphene in the simulation, the SCBC is a native, surface-based modeling method. It avoids errors from the finite-thickness approximation, as well as the resulting extrafine meshing [32].

Funding. National Natural Science Foundation of China (NSFC) (11604276, 61601393, 11501481); Key Scientific Project of Fujian Province in China (2015H0039).

REFERENCES

1. K. S. Novoselov, V. I. Fal'ko, L. Colombo, P. R. Gellert, M. G. Schwab, and K. Kim, "A roadmap for graphene," Nature **490**, 192–200 (2012).
2. A. N. Grigorenko, M. Polini, and K. S. Novoselov, "Graphene plasmonics," Nat. Photonics **6**, 749–758 (2012).
3. F. J. G. de Abajo, "Graphene plasmonics: challenges and opportunities," ACS Photon. **1**, 135–152 (2014).
4. L. Ju, B. S. Geng, J. Horng, C. Girit, M. Martin, Z. Hao, H. A. Bechtel, X. G. Liang, A. Zettl, Y. R. Shen, and F. Wang, "Graphene plasmonics for tunable terahertz metamaterials," Nat. Nanotechnol. **6**, 630–634 (2011).
5. J. Christensen, A. Manjavacas, S. Thongrattanasiri, F. H. L. Koppens, and F. J. G. de Abajo, "Graphene plasmon waveguiding and hybridization in individual and paired nanoribbons," ACS Nano **6**, 431–440 (2012).
6. D. Rodrigo, O. Limaj, D. Janner, D. Etezadi, F. J. G. de Abajo, V. Pruneri, and H. Altug, "Mid-infrared plasmonic biosensing with graphene," Science **349**, 165–168 (2015).
7. Z. Fei, G. O. Andreev, W. Bao, L. M. Zhang, A. S. McLeod, C. Wang, M. K. Stewart, Z. Zhao, G. Dominguez, M. Thiemens, M. M. Fogler, M. J. Tauber, A. H. Castro-Neto, C. N. Lau, F. Keilmann, and D. N. Basov, "Infrared nanoscopy of Dirac plasmons at the graphene-SiO_2 interface," Nano Lett. **11**, 4701–4705 (2011).
8. W. Gao, G. Shi, Z. Jin, J. Shu, Q. Zhang, R. Vajtai, P. M. Ajayan, J. Kono, and Q. Xu, "Excitation and active control of propagating surface plasmon polaritons in graphene," Nano Lett. **13**, 3698–3702 (2013).
9. X. Zhu, W. Yan, P. U. Jepsen, O. Hansen, N. A. Mortensen, and S. Xiao, "Experimental observation of plasmons in a graphene monolayer resting on a two-dimensional subwavelength silicon grating," Appl. Phys. Lett. **102**, 131101 (2013).
10. P. A. D. Gonçalves and N. M. R. Peres, *An Introduction to Graphene Plasmonics* (World Scientific, 2016).
11. F. Ramos-Mendieta, J. A. Hernandez-Lopez, and M. Palomino-Ovando, "Transverse magnetic surface plasmons and complete absorption supported by doped graphene in Otto configuration," AIP Adv. **4**, 067125 (2014).
12. C. H. Gan, "Analysis of surface plasmon excitation at terahertz frequencies with highly doped graphene sheets via attenuated total reflection," Appl. Phys. Lett. **101**, 111609 (2012).
13. Y. V. Bludov, M. I. Vasilevskiy, and N. M. R. Peres, "Mechanism for graphene-based optoelectronic switches by tuning surface plasmon-polaritons in monolayer graphene," Europhys. Lett. **92**, 68001 (2010).
14. Y. V. Bludov, M. I. Vasilevskiy, and N. M. R. Peres, "Tunable graphene-based polarizer," J. Appl. Phys. **112**, 084320 (2012).
15. X. Dai, L. Jiang, and Y. Xiang, "Tunable THz angular/frequency filters in the modified Kretschmann-Raether configuration with the insertion of single layer graphene," IEEE Photon. J. **7**, 5500808 (2015).
16. H. Wang, J. Wu, J. Guo, L. Jiang, Y. Xiang, and S. Wen, "Low-threshold optical bistability with multilayer graphene-covering Otto configuration," J. Phys. D **49**, 255306 (2016).
17. K. Liu, C. R. Ye, S. Khan, and V. J. Sorger, "Review and perspective on ultrafast wavelength-size electro-optic modulators," Laser Photon. Rev. **9**, 172–194 (2015).
18. P. Q. Liu, F. Valmorra, C. Maissen, and J. Faist, "Electrically tunable graphene anti-dot array terahertz plasmonic crystals exhibiting multi-band resonances," Optica **2**, 135–140 (2015).
19. C. Zeng, Y. Cui, and X. Liu, "Tunable multiple phase-coupled plasmon-induced transparencies in graphene metamaterials," Opt. Express **23**, 545–551 (2015).
20. Z. Wei, X. Li, J. Yin, R. Huang, Y. Liu, W. Wang, H. Liu, H. Meng, and R. Liang, "Active plasmonic band-stop filters based on graphene metamaterial at THz wavelengths," Opt. Express **24**, 14344–14351 (2016).
21. Y. Zhang, T. Li, B. Zeng, H. Zhang, H. Lv, X. Huang, W. Zhang, and A. K. Azad, "A graphene based tunable terahertz sensor with double Fano resonances," Nanoscale **7**, 12682–12688 (2015).
22. Y. Zhang, T. Li, Q. Chen, H. Zhang, J. F. O'Hara, E. Abele, A. J. Taylor, H.-T. Chen, and A. K. Azad, "Independently tunable dual-band perfect absorber based on graphene at mid-infrared frequencies," Sci. Rep. **5**, 18463 (2015).
23. Y. Chen, J. Yao, Z. Song, L. Ye, G. Cai, and Q. H. Liu, "Independent tuning of double plasmonic waves in a free-standing graphene-spacer-grating-spacer-graphene hybrid slab," Opt. Express **24**, 16961–16972 (2016).
24. Y. Liu and R. F. Willis, "Plasmon-phonon strongly coupled mode in epitaxial graphene," Phys. Rev. B **81**, 081406 (2010).

25. T. Zhan, X. Shi, Y. Dai, X. Liu, and J. Zi, "Transfer matrix method for optics in graphene layers," J. Phys. Condens. Matter **25**, 215301 (2013).
26. A. Vakil and N. Engheta, "Transformation optics using graphene," Science **332**, 1291–1294 (2011).
27. N. Liu, G. Cai, L. Ye, and Q. H. Liu, "The efficient mixed FEM with the impedance transmission boundary condition for graphene plasmonic waveguides," J. Lightwave Technol. **34**, 5363–5370 (2016).
28. E. H. Hwang, S. Adam, and S. Das Sarma, "Carrier transport in two-dimensional graphene layers," Phys. Rev. Lett. **98**, 186806 (2007).
29. W. Gao, J. Shu, C. Qiu, and Q. Xu, "Excitation of plasmonic waves in graphene by guided-mode resonances," ACS Nano **6**, 7806–7813 (2012).
30. G. Pirruccio, L. Martín Moreno, G. Lozano, and J. G. Rivas, "Coherent and broadband enhanced optical absorption in graphene," ACS Nano **7**, 4810–4817 (2013).
31. M. Jablan, H. Buljan, and M. Soljačić, "Plasmonics in graphene at infrared frequencies," Phys. Rev. B **80**, 245435 (2009).
32. N. K. Emani, D. Wang, T. F. Chung, L. J. Prokopeva, A. V. Kildishev, V. M. Shalaev, Y. P. Chen, and A. Boltasseva, "Plasmon resonance in multilayer graphene nanoribbons," Laser Photon. Rev. **9**, 650–655 (2015).